Gamow-Teller unit cross sections of the (p,n) reaction at 198 and 297 MeV on medium-heavy nuclei

M. Sasano,[1,*] H. Sakai,[1] K. Yako,[1] T. Wakasa,[2] S. Asaji,[2] K. Fujita,[2] Y. Fujita,[3] M. B. Greenfield,[7] Y. Hagihara,[2] K. Hatanaka,[4] T. Kawabata,[6] H. Kuboki,[5] Y. Maeda,[9] H. Okamura,[4] T. Saito,[1] Y. Sakemi,[8] K. Sekiguchi,[5] Y. Shimizu,[6] Y. Takahashi,[1] Y. Tameshige,[4] and A. Tamii[4]

[1]*Department of Physics, The University of Tokyo, Bunkyo, Tokyo 113-0033, Japan*
[2]*Department of Physics, Kyushu University, Higashi, Fukuoka 812-8581, Japan*
[3]*Department of Physics, Osaka University, Toyonaka, Osaka 560-0043, Japan*
[4]*Research Center for Nuclear Physics, Osaka University, Ibaraki, Osaka 567-0047, Japan*
[5]*The Institute of Physical and Chemical Research, Wako, Saitama 351-0198, Japan*
[6]*Center for Nuclear Study, The University of Tokyo, Bunkyo, Tokyo 113-0033, Japan*
[7]*Department of Physics, International Christian University, Mitaka, Tokyo 181-8585, Japan*
[8]*Cyclotron and Radioisotope Center, Tohoku University, Aoba-ku, Sendai 980-8578, Japan*
[9]*Department of Applied Physics, University of Miyazaki, Kibanadai-nishi, Miyazaki-shi 889-2192, Japan*

(Received 11 September 2008; published 3 February 2009)

Gamow-Teller (GT) unit cross sections, $\hat{\sigma}_{\mathrm{GT}}$, are obtained at 198 and 297 MeV by measuring the double differential cross sections at 0° for the (p,n) reaction on ^{58}Ni, ^{70}Zn, ^{114}Cd, ^{118}Sn, and ^{120}Sn. The mass dependence of $\hat{\sigma}_{\mathrm{GT}}$ and the ratio of $\hat{\sigma}_{\mathrm{GT}}$ to the Fermi unit cross section, $\hat{\sigma}_{\mathrm{F}}$, (R^2) are also derived in the mass region of $58 \leqslant A \leqslant 120$. The $\hat{\sigma}_{\mathrm{GT}}$ value for ^{90}Zr at 297 MeV interpolated using the A-dependence obtained herein agrees with that used in a previous analysis where the GT transition strength over a wide energy region up to the continuum was discussed. However, the deduced ^{64}Ni $\hat{\sigma}_{\mathrm{GT}}$ value at 198 MeV is 20% smaller than that obtained from the analysis of a previous (n,p) measurement. The present R^2 values in the mass region heavier than ^{42}Ca are larger than those in the region up to ^{42}Ca and increase as a function of A.

DOI: 10.1103/PhysRevC.79.024602 PACS number(s): 25.40.Kv

I. INTRODUCTION

Nuclear spin and isospin processes have attracted much attention because their collectivities are closely related to the properties of nuclear interactions in the spin-isospin channel [1,2]. Among them, the Gamow-Teller (GT) transition is the simplest because both spin and isospin transfers change their respective quantum numbers by one unit, but the other quantum numbers remain the same. Collective aspects of the GT transition have been studied extensively for light to heavy nuclei over a wide excitation-energy region including the GT giant resonance (GTGR) [3–5]. In particular, fp-shell nuclei [6–8] have been intensely studied due to their astrophysical significance. Knowledge of weak processes in stellar cores, especially the GT transition, is essential to the understanding of stellar-core evolution, which leads to supernovae [9].

The β-decay provides the most reliable experimental source for the GT transition strength, B(GT). Unfortunately, GT states of interest are normally located in a high excitation-energy region which is inaccessible by the β-decay. Thus, the (p,n) reaction at intermediate energies ($T_p \geqslant 100$ MeV) is a powerful probe to explore such relatively high excitation-energy regions. When this reaction excites a GT state, angular momentum is not transferred from the target nucleus to the projectile ($\Delta L = 0$), which implies that the angular distribution of the differential cross section peaks at 0°. The GT cross section measured at 0°, $\sigma_{\mathrm{GT}}(0^\circ)$, is expected to be related to the corresponding B(GT) value through the proportionality,

$$\sigma_{\mathrm{GT}}(0^\circ) = \hat{\sigma}_{\mathrm{GT}} F(q,\omega) B(\mathrm{GT}), \tag{1}$$

where the proportionality factor, $\hat{\sigma}_{\mathrm{GT}}$, which is called the "GT unit cross section," depends on the incident energy and target mass [10]. Herein the $\hat{\sigma}_{\mathrm{GT}}$ values for a variety of masses are determined. The definition of B(GT) is often a source of confusion. Herein $B(\mathrm{GT}) \equiv |\langle f || \sum_k \vec{\sigma}_k t_k^- || i \rangle|^2 / (2J_i + 1)$, where $|i\rangle$ and $|f\rangle$ are the initial and final states, respectively, $\sum_k \vec{\sigma}_k t_k^-$ is the so-called GT operator, the subscript, k, runs over all the neutron orbits of the target nucleus, $\vec{\sigma}_k$ is the usual Pauli spin operator, t_k^- is the isospin lowering operator, and J_i is the total spin of the initial state. $F(q,\omega)$, which gives the dependence of σ_{GT} on the momentum (q) and energy (ω) transfers, is defined as the ratio of the cross section at finite (q,ω) values to that at $(q = \omega = 0)$ and can be reliably calculated by employing a distorted wave impulse approximation (DWIA). On the other hand, theoretical estimates of $\hat{\sigma}_{\mathrm{GT}}$ suffer from uncertainties in the relative strength of the isovector part of the NN interactions, the effect of distortions, etc. Hence, to extract reliable B(GT) values, $\hat{\sigma}_{\mathrm{GT}}$ must be calibrated empirically for every incident-energy and mass region.

A $\hat{\sigma}_{\mathrm{GT}}$ value can be determined by measuring the cross section at 0° for a GT transition whose B(GT) value is deduced from a ft-value for the corresponding β-decay. In most cases, an accurate ft-value exists only for the transition between the ground states. Therefore, the transition to the ground state must be separated from those to the excited states. However, the relatively poor energy resolution in (p,n) experiments where kinetic energies of neutrons are determined by the time-of-flight (TOF) method

*sasano@nucl.phys.s.u-tokyo.ac.jp; http://nucl.phys.s.u-tokyo.ac.jp/sasano

often hampers the separation. This is a particularly serious problem in determining $\hat{\sigma}_{\rm GT}$ values in medium-heavy to heavier nuclei because the level density of low-lying states is relatively high. In addition, for a fixed flight path, the TOF decreases as T_p increases. Thus, for a given time resolution, the energy resolution decreases with increasing T_p, which makes it increasingly difficult to resolve the low-lying states. Therefore, in the incident-energy region of $T_p \geqslant 200$ MeV, only one nucleus heavier than ^{15}N, namely ^{42}Ca, has been studied [10], though, for energies of $T_p \leqslant 160$ MeV, the $\hat{\sigma}_{\rm GT}$ values have been systematically determined over a wide mass range from ^{6}Li to ^{162}Dy [10]. Nevertheless, many studies of the GT transition in medium-heavy nuclei [4–8] have been conducted in the region of $T_p = 200$–300 MeV, where the distortion is least [11] and thus, GT transitions can be cleanly observed in the 0° spectrum.

In this study, we measured the double differential cross sections for the (p,n) reaction at 0° for five medium-heavy nuclei ^{58}Ni, ^{70}Zn, ^{114}Cd, ^{118}Sn, and ^{120}Sn at 198 and 297 MeV, and derived the $\hat{\sigma}_{\rm GT}$ values for the ground-state transitions with known B(GT) values from the β-decay [12–16]. This work presents the first systematic study of such a wide range of masses ($A = 58$–120) at these incident energies. An energy resolution of 0.3 and 0.5 MeV was achieved at 198 and 297 MeV, respectively, by employing the new neutron detection system NPOL3 [17]. We also obtained the Fermi unit cross section, $\hat{\sigma}_{\rm F}$, [10] and the ratio of $\hat{\sigma}_{\rm GT}$ to $\hat{\sigma}_{\rm F}$, the so-called R^2 value [10], which is frequently used to deduce B(GT) when the experimental $\hat{\sigma}_{\rm GT}$ value is unavailable.

II. EXPERIMENT

The (p,n) experiments at 198 and 297 MeV were performed using the neutron time-of-flight (NTOF) facility [18] at the Research Center for Nuclear Physics, Osaka University where a proton beam was accelerated up to 297 MeV by an azimuthally-varying-field (AVF) cyclotron and a Ring cyclotron. In the injection line from the AVF to the Ring cyclotron, one out of five beam pulses was selected to reduce wraparound events caused by slow neutrons. The effective separation between beam pulses was about 370 and 320 ns in the 198- and 297-MeV experiments, respectively, while the average beam intensity was about 100 nA on a target.

Targets were enriched self-supporting metallic foils of ^{58}Ni (>99.5%), ^{70}Zn (85%), ^{114}Cd (99.2%), ^{118}Sn (95%), and ^{120}Sn(>99.5%), which had thicknesses of 99 ± 2 mg/cm^2, 9.3 ± 0.3 mg/cm^2, 11.8 ± 0.4 mg/cm^2, 100 ± 2 mg/cm^2, and 160 ± 3 mg/cm^2, respectively. Only ^{58}Ni and ^{120}Sn targets were used in the 198-MeV experiment.

In the 297-MeV experiment, neutrons were detected using the neutron detection system NPOL3 [17] positioned at approximately 100 m from the target. NPOL3, which was originally designed for neutron-polarimetry measurements, consisted of three scintillation detector planes. The first two planes (HD1 and HD2) were the neutron polarization analyzer, and the last plane (NC) was the catcher of doubly scattered neutrons and recoiled protons. Each plane subtended a solid angle of about 0.1 msr. In this study, only HD1 and HD2 were used as the neutron detectors. HD1 and HD2 each consisted of ten sets of plastic scintillation bars, which measured $100 \times 10 \times 5$ cm^3. The events under the condition that a neutron was detected in HD1 and a recoiled proton from HD1 was caught in HD2 were analyzed. This coincidence between HD1 and HD2 effectively reduced the tail of the peak in the TOF spectrum as well as improved the energy resolution (see Ref. [17] for details). The scintillation light output was calibrated using 4.4-MeV γ rays from a ^{241}Am-^{9}Be source and cosmic rays (mostly $\mu^{\pm}$). Here the threshold levels for the light output of HD1 and HD2 were set at 6 and 10 MeV electron equivalent energy, respectively. As to the ^{118}Sn target, the angular distribution from $\theta = 0°$–12° was also measured to extract the GT cross section from the observed bump near $E_x = 0$ MeV in which the contributions from low-lying multipole excitations other than $\Delta L = 0$ are expected.

In the 198-MeV experiment, neutrons were detected by a prototype of NPOL3, which consisted of two scintillation detector planes. The first one consisted of four plastic scintillation bars with a thickness of 5 cm and subtended a solid angle of about 0.04 msr. The second one was NC of NPOL3. The coincidence events between the two planes were analyzed in a similar manner as in the 297-MeV experiment.

The neutron TOF was obtained from the timing pulses generated from the anode signals of the PMT's attached to the both ends of the scintillation bars and the rf signal from the cyclotron. The absolute TOF scale was calibrated using the $^{\rm nat}$C(p,n) spectrum at 0°. Figure 1 shows the TOF spectrum at 300 MeV with the two prominent peaks associated with neutrons from the ^{13}C$(p,n)^{13}$N(3.50 MeV; $Q = -6.50$ MeV) and ^{12}C$(p,n)^{12}$N(g.s.; $Q = -18.12$ MeV) reactions. Examining the relative peak positions in the TOF spectrum indicated that the mean energies of the incident protons were 197.6 ± 0.3 and 297.4 ± 0.3 MeV for nominal 200- and 300-MeV beams, respectively. After correcting for the effect of the energy loss in the target, the overall time resolution determined from the full width at half maximum (FWHM) of the ^{12}N(g.s.) peak was 230 ps, which corresponds to an energy resolution of approximately 0.3 and 0.5 MeV at 198 and 297 MeV, respectively. This energy resolution includes contributions from the intrinsic time resolution of the detectors as well as the time spread of the beam.

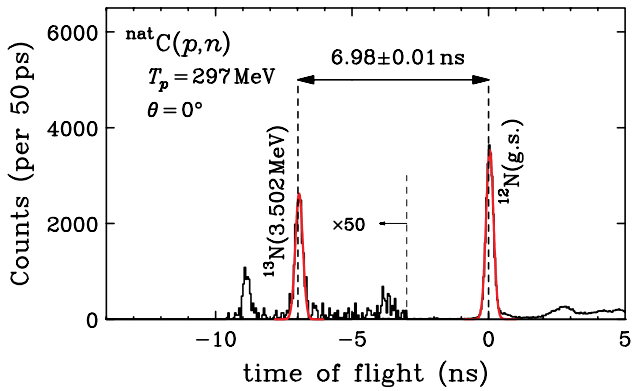

FIG. 1. (Color online) TOF spectrum for the $^{\rm nat}$C(p,n) reaction at $T_p = 297$ MeV. Peaks due to the ^{13}C$(p,n)^{13}$N(3.502 MeV) and ^{12}C$(p,n)^{12}$N(g.s.) reactions are fitted with Gaussians.

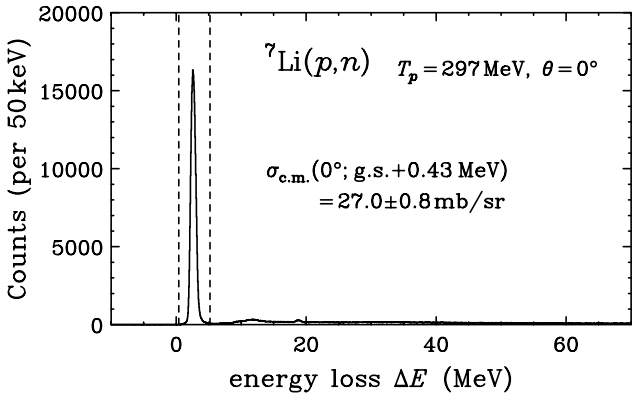

FIG. 2. Energy-loss spectrum for the ^{7}Li(p,n) reaction at T_p = 297 MeV and $\theta = 0^\circ$. Events between two vertical dashed lines are due to the ^{7}Li$(p,n)^7$Be(g.s. + 0.43 MeV) reaction.

The neutron-detection efficiency was determined via the ^{7}Li$(p,n)^7$Be(g.s. + 0.43 MeV) reaction at 0° [19]. The target was a self-supporting metallic foil enriched to 99.971% ^{7}Li with a thickness of 2.62 ± 0.08 mm. Figure 2 shows the spectrum at 297 MeV where the peak sandwiched between two vertical dashed lines is that of the ^{7}Li$(p,n)^7$Be(g.s. + 0.43 MeV) reaction at 0°. Then using the yield and the known cross section of 27.0 ± 0.8 mb/sr in the center of the mass frame of the reaction [19], the obtained neutron-detection efficiency was $(1.90 \pm 0.09) \times 10^{-2}$ and $(1.45 \pm 0.07) \times 10^{-2}$ at 198 and 297 MeV, respectively. The uncertainty is mainly due to the systematic errors, which include the uncertainties in the beam current (±2%), the target thickness (±3%), and the cross section (±3%).

III. RESULTS AND ANALYSIS

Figures 3 and 4 show the double differential cross sections as a function of the reaction energy loss, $\Delta E \equiv T_p - T_n$, for the (p,n) reaction at 198 and 297 MeV, respectively, on ^{58}Ni, ^{70}Zn, ^{114}Cd, ^{118}Sn, and ^{120}Sn. The bump around $E_x = 0$ MeV observed in each spectrum is dominated by the GT transition to the ground state except for that in the ^{58}Ni(p,n) spectra, to which a significant amount of the Fermi transition to the isobaric analog state (IAS) at 203 keV also contributes.

To obtain the differential cross section for the GT transition to the ground state, which has a known B(GT) value from β-decay, each spectrum was fitted in a low energy-loss region. The shape of each peak was assumed to be a Gaussian. The left panels of Figs. 5 and 6 show the excitation-energy spectra with the fitted curves, while Table I summarizes the 0° differential cross sections, $\sigma_{\rm GT}(0^\circ)$. Each error was the quadratic sum of the uncertainties due to the fitting and other systematic uncertainties in the target thicknesses (±3%), the ^{7}Li target thickness (±3%), the integrated current (±2%), the effect of the ^{120}Sn contaminant in the ^{118}Sn target (±3%), and the contributions from the multipole excitations (±4% for ^{118}Sn and ^{120}Sn), which are explained below.

In the ^{58}Ni(p,n) spectra, the two bumps in the energy region of $-1.0 \leqslant E_x \leqslant 1.7$ MeV were fitted using the excitation-energy data listed in Table II [20]. Because the calibration of the energy scale is essential to decompose these two bumps into individual peaks, the energy scale was determined to an

TABLE II. Excitation energies and J^π values on ^{58}Cu included in the fitting of the ^{58}Ni(p,n) spectra. Excitation energies are from Ref. [20].

Excitation energy (kev)	J^π
0	1^+
202.6 ± 0.3	0+
443.7 ± 0.2	(3^+)
1051.0 ± 0.3	(1^+)
1427.8 ± 0.3	2^+
1651.6 ± 0.3	2^+

TABLE I. Differential cross sections, kinetic correction factors, and B(GT) values used to determine the $\hat{\sigma}_{\rm GT}$ values. In the ^{114}Cd case, the B(GT) and $\hat{\sigma}_{\rm GT}$ values should be updated as a more reliable ft value becomes available (see the text for details).

Nuclide	T_p (MeV)	Gamow-Teller				Fermi				R^2
		$\sigma_{\rm GT}(0^\circ)$ (mb/sr)	$F(q,\omega)$	B(GT)	$\hat{\sigma}_{\rm GT}$ (mb/sr)	$\sigma_{\rm F}(0^\circ)$ (mb/sr)	$F(q,\omega)$	B(F)	$\hat{\sigma}_{\rm F}$ (mb/sr)	
^{58}Ni	198	0.71 ± 0.06	1.00	0.155 ± 0.001[a]	4.56 ± 0.46	0.60 ± 0.08	1.00	2	0.30 ± 0.04	15 ± 3
	297	0.67 ± 0.04	1.01		4.27 ± 0.26	0.46 ± 0.03	1.01		0.226 ± 0.016	19 ± 1
^{70}Zn	297	0.97 ± 0.12	1.01	0.221 ± 0.025[b]	4.33 ± 0.71	1.8 ± 0.2	1.01	10	0.18 ± 0.02	25 ± 3
^{114}Cd	297	0.80 ± 0.09	1.03	0.14 ± 0.05[c]	5.5 ± 2.1	1.7 ± 0.2	1.01	18	0.088 ± 0.010	63 ± 24
^{118}Sn	297	1.03 ± 0.08	1.04	0.343 ± 0.010[d]	2.88 ± 0.24	2.04 ± 0.13	1.07	18	0.106 ± 0.007	27 ± 2
^{120}Sn	198	1.01 ± 0.12	1.04	0.342 ± 0.008[e]	2.84 ± 0.36	3.34 ± 0.27	1.04	20	0.161 ± 0.012	18 ± 3
	297	0.98 ± 0.07	1.03		2.78 ± 0.16	2.36 ± 0.14	1.07		0.110 ± 0.007	25 ± 4

[a]From Ref. [12].
[b]From Ref. [13].
[c]From Ref. [14].
[d]From Ref. [15].
[e]From Ref. [16].

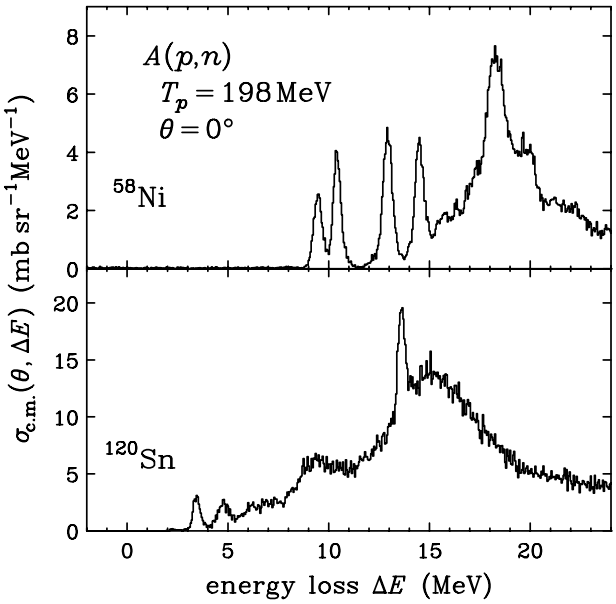

FIG. 3. Double differential cross sections for the (p,n) reaction at 198 MeV on ^{58}Ni and ^{120}Sn as a function of energy loss of the reaction.

accuracy of 2 keV from the analysis of the ^{nat}C(p,n) spectrum mentioned above.

In the ^{70}Zn spectrum, the bump around $E_x = 0$ MeV was fitted by assuming two peaks, one for the ground state and another for an excited state. Because the peak position for the excited state is not well known, it was adjusted to improve the quality of the fit. In the ^{114}Cd spectrum, the bump around $E_x = 0$ MeV was fitted by assuming a single peak. Similarly, in the ^{118}Sn and ^{120}Sn spectra, the bump around $E_x = 0$ MeV was fitted assuming a single peak. The obtained 0° differential cross sections were 1.19 ± 0.08 and 1.10 ± 0.07 mb/sr for the ^{118}Sb(g.s.) and ^{120}Sb(g.s.) at 297 MeV, respectively, and 1.13 ± 0.12 mb/sr for the ^{120}Sb(g.s.) at 198 MeV.

Figure 7 shows the angular distribution for the fitted peak of ^{118}Sb for the scattering angles in the center of mass system θ between 0° and 12°. The differential cross section has its maximum at 0°, which indicates the dominance of the GT ($\Delta L = 0$) component. However, the cross section decreases very slowly with the scattering angle compared to that for a pure GT state, which implies the existence of the unresolved excited states with higher ΔL, e.g., $J^\pi = (2)^-(\Delta L = 1) : 31$ keV, $3^+(\Delta L = 2) : 51$ keV, $(4)^+(\Delta L = 4) : 82$ keV, $2^+(\Delta L = 2) : 166$ keV, and $3^-(\Delta L = 3) : 270$ keV [21]. Therefore the 0° differential cross section was corrected for the contributions from higher ΔL using a multipole decomposition (MD) analysis. The MD analysis was performed by fitting the angular distribution with the function,

$$\sigma^{\rm calc}(\theta) = \sum_{\Delta L=0}^{4} a_{\Delta L}\sigma^{\rm calc}_{\Delta L}(\theta), \qquad (2)$$

where $a_{\Delta L}$ and $\sigma^{\rm calc}_{\Delta L}$ are the fitting parameter and the angular distribution calculated by DWIA, respectively, and correspond to the contribution from each ΔL component. Here χ^2 is

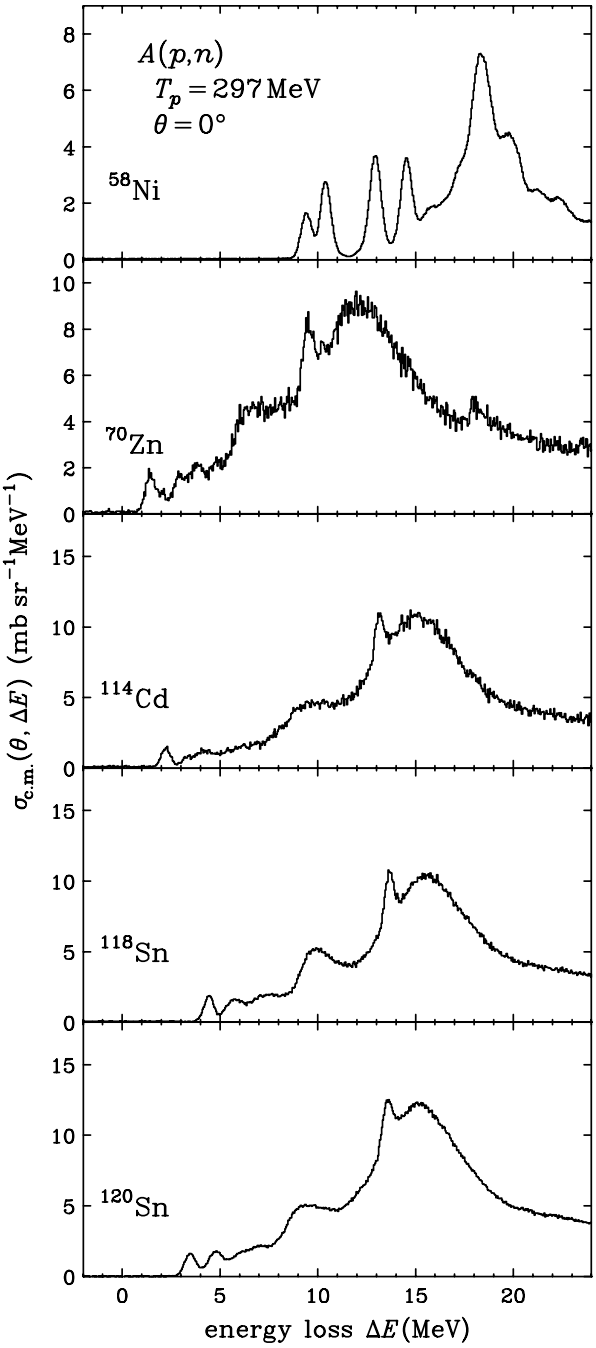

FIG. 4. Double differential cross sections for the (p,n) reaction at 297 MeV on ^{58}Ni, ^{70}Zn, ^{114}Cd, ^{118}Sn, and ^{120}Sn as a function of energy loss of the reaction.

defined as

$$\chi^2 = \sum_{i=1}^{7} \left(\frac{\sigma^{\rm exp}(\theta_i) - \sigma^{\rm calc}(\theta_i)}{\delta\sigma(\theta_i)} \right)^2, \qquad (3)$$

where $\delta\sigma(\theta_i)$ is the statistical uncertainty of each data point ($\sim$10%).

The DWIA calculations were performed using the computer code DW81 [22] with effective interactions at 325 MeV by Franey and Love [23] and the optical potential by Cooper

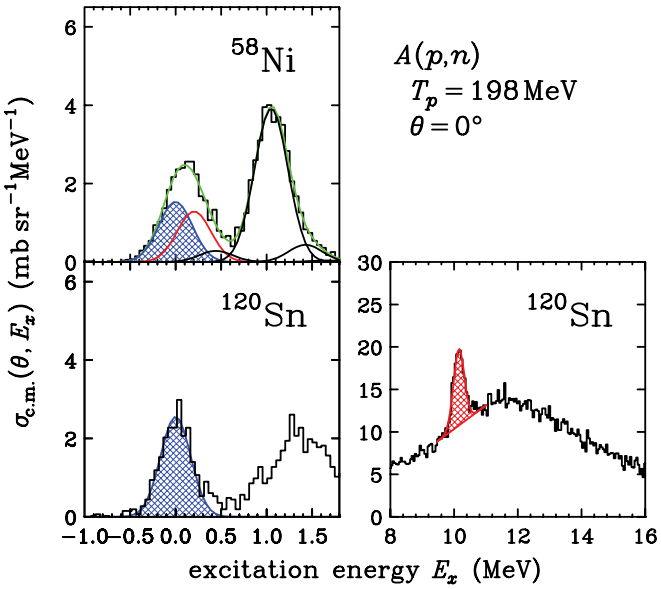

FIG. 5. (Color online) Excitation-energy spectra for the (p,n) reaction at 198 MeV on ^{58}Ni and ^{120}Sn with fitted curves for each individual peak for the low-lying discrete states (left windows) and IAS (right windows). In the ^{58}Ni(p,n) spectrum, the shaded peak at 0 MeV is the ground state (1^+) and the neighboring peak at 203 keV is IAS.

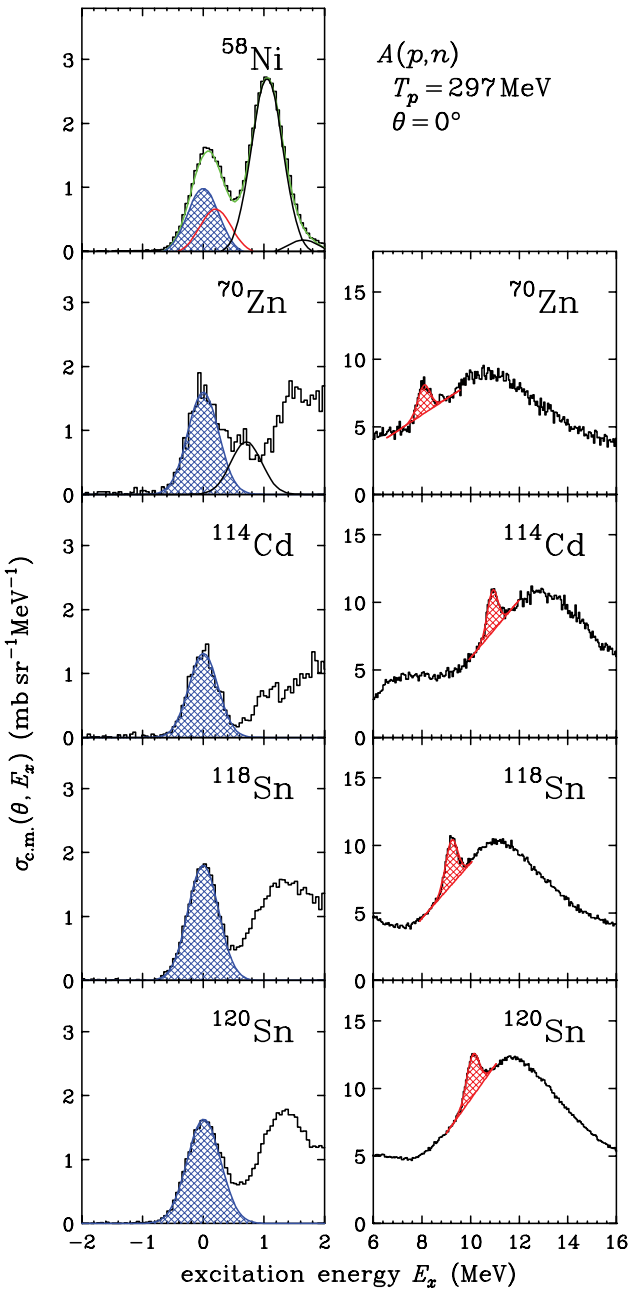

FIG. 6. (Color online) Excitation-energy spectra for the (p,n) reaction at 297 MeV on ^{58}Ni, ^{70}Zn, ^{114}Cd, ^{118}Sn, and ^{120}Sn with fitted curves for each individual peak for the low-lying discrete states (left windows) and IAS (right windows). In the ^{58}Ni(p,n) spectrum, the shaded peak at 0 MeV is the ground state (1^+) and peak at 203 MeV is IAS.

and Hama [24] (without the Coulomb interaction for the exit channel). Herein, assuming that the ^{90}Zr core is not excited, the active proton-particles and neutron-holes were restricted to the $0g\frac{9}{2}$, $1d\frac{5}{2}$, $0g\frac{7}{2}$, $2s\frac{1}{2}$, $1d\frac{3}{2}$, or $0h\frac{11}{2}$ shells and to the $1d\frac{5}{2}$, $0g\frac{7}{2}$, $2s\frac{1}{2}$, $1d\frac{3}{2}$, or $0h\frac{11}{2}$ shells, respectively. Each radial wave function was generated from the Woods-Saxon (WS) potential [25] whose depth was adjusted to reproduce the binding energy.

Figure 7 shows the result of the MD analysis. The extracted $\Delta L = 0$ cross section at 0° was $1.03 \pm 0.07 \pm 0.04$ mb/sr. Here the central value was defined as the value where the χ^2 value per degree of freedom becomes the smallest ($\chi^2_{\rm min}/2 = 0.5$) among all possible combinations of the $1p1h$ configurations. The first uncertainty was the result of the quadratic sum of the fitting uncertainty and other systematic errors in the total 0° cross section. The second one was the error associated with the MD analysis, which is defined below. Each combination of the $1p1h$ configurations gave a different $\Delta L = 0$ cross section. Thus, the error was defined as the largest deviation of the $\Delta L = 0$ cross section from the central value for the combinations in the range of $\chi^2_{\rm min} < \chi^2 < \chi^2_{\rm min} + 1$. The obtained $\Delta L \neq 0$ cross section at 0° was about $11 \pm 4\%$ of the cross section of the entire peak. The main contribution was due to the $\Delta L = 2$ component, which is consistent with the result of the high energy resolution ^{118}Sn(^{3}He,t) measurement [26].

In regard to the ^{120}Sn(p,n) spectrum, an angular distribution was not measured. Therefore, the $\Delta L \neq 0$ cross section at 0° must be deduced by means other than the MD analysis. In this work, we assumed the contribution from the $\Delta L \neq 0$ cross section in ^{120}Sb as $11 \pm 4\%$, expecting that the nuclear structure of ^{120}Sb is similar to that of ^{118}Sb. Thus, the determined cross sections were 1.01 ± 0.12 and 0.98 ± 0.07 mb/sr at 198 and 297 MeV, respectively.

The differential cross sections for the Fermi transitions to the IAS's were obtained by fitting the spectra in the GTGR region around the IAS peaks. The exception was the ^{58}Ni(p,n) spectra, because the IAS peak at 203 keV was already obtained when the cross section to the ground state was derived. The

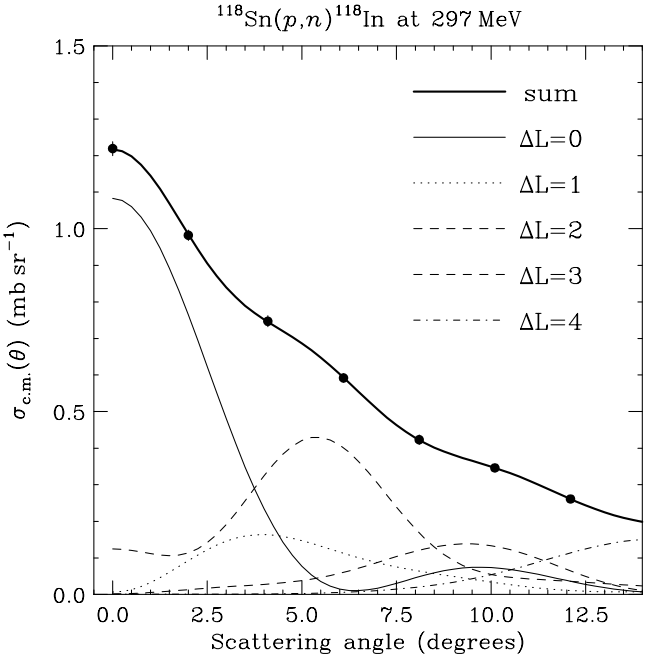

FIG. 7. Angular distribution of the differential cross sections for ^{118}Sn$(p,n)^{118}$Sb(g.s.) with the results of the MD analysis. Thick curve shows the sum of the $\Delta L = 0$–4 components. Angular distributions of each ΔL component are also shown.

right panels of Figs. 5 and 6 show the excitation-energy spectra with the fitted curves when the physical background below the IAS peak is assumed to be a linear function of the excitation energy within the relevant energy region. Table I summarizes the obtained cross sections, $\sigma_{\rm F}(0^\circ)$.

From the obtained differential cross section for a GT transition to the ground state, the $\hat{\sigma}_{\rm GT}$ value was derived using Eq. (1). Here the B(GT) value was obtained by comparing the ft value of the corresponding β-decay with the averaged $\mathcal{F}t$ value (see Ref. [27] for the definition of $\mathcal{F}t$) for superallowed Fermi transitions, $\overline{\mathcal{F}t}$, as

$$B(\mathrm{GT}) = \frac{2J_f+1}{2J_i+1}\frac{C}{(G_{\rm A}/G_{\rm V})^2 ft}, \tag{4}$$

where $C \equiv B(\mathrm{F}) \times \overline{\mathcal{F}t} = 2 \times (3072.7 \pm 0.8)$ s [27] and $G_{\rm A}/G_{\rm V} = 1.2695 \pm 0.0029$ [28] is the ratio of axial-vector to vector coupling constants of the neutron β decay. The J_i and J_f values represent the total spins of the initial and final states of the target nucleus, respectively. The $F(q,\omega)$ value was derived by the DWIA calculations with the parameters mentioned above.

The solid circles in Figs. 8 and 9 show the derived $\hat{\sigma}_{\rm GT}$ values at 198 and 297 MeV as a function of A. Table I also summarizes the derived values. The error bars represent the results of the quadratic sum of the fitting and systematic errors. The fitting error is mainly due to the statistical error. The systematic error includes the uncertainties in the cross sections (±6–8%), B(GT) by β-decay (±0.6%, ±11%, ±33%, ±2%, and ±2% for ^{58}Ni, ^{70}Zn, ^{114}Cd, ^{118}Sn, and ^{120}Sn, respectively), and $F(q,\omega)$ (±0.3%).

The reliability of the present $\hat{\sigma}_{\rm GT}$ values depends on that of the ft values used herein. In the ^{114}Cd case, however, it is problematic to use the ft value evaluated in Ref. [14] because there exist two conflicting data for the branching ratio of the transition from ^{114}In to ^{114}Cd. In Ref. [14], the evaluator adopts the electron-capture branching ratio of $0.46 \pm 0.15\%$, which is deduced from the positron-emission branching ratio of $0.0035 \pm 0.0011\%$ in Ref. [29] by using the theoretical ratio of the electron-capture to position-emission intensities [30] according to the general policy of Nuclear Data Sheets for the evaluation of the β-decay rate probabilities. On the other hand, in the original paper [29], the branching ratio for the K-electron capture is deduced to be 1.9% with no error. If one reevaluates the ft value in Ref. [14] by using the value of 1.9%, the B(GT) value becomes larger and, consequently, the $\hat{\sigma}_{\rm GT}$ value of ^{114}Cd smaller by a factor of four, though the uncertainties are not derived. Thus, the $\hat{\sigma}_{\rm GT}$ value of ^{114}Cd should be updated as a more reliable ft value becomes available.

The $\hat{\sigma}_{\rm F}$ values were derived from the Fermi cross sections using the equation,

$$\hat{\sigma}_{\rm F} = \sigma_{\rm F}(0^\circ)/\{(N-Z)F(q,\omega)\}. \tag{5}$$

Our results, which are a function of A, are shown as solid circles in Figs. 8 and 9, and are summarized in Table I. The error bars are the results of the quadratic sum of the fitting and systematic errors. Each systematic error includes the systematic uncertainties in the cross sections (±6%) and $F(q,\omega)$ (±0.3%).

IV. DISCUSSION

A. A-dependence of $\hat{\sigma}_{\rm GT}$ and $\hat{\sigma}_{\rm F}$

The mass dependences of $\hat{\sigma}_{\rm GT}$ and $\hat{\sigma}_{\rm F}$ at 198 and 297 MeV were derived by fitting the present data points. Herein we assumed that the A-dependence can be written as a smooth function of A,

$$\hat{\sigma}(A) = N\exp(-xA^{\frac{1}{3}}), \tag{6}$$

according to the parametrization in Ref. [10]. Here N represents the unit cross section at $A = 0$. Therefore, Eq. (6) is not practical for medium-heavy nuclei. Hence, we chose $A = 90$ as the central value and rewrote Eq. (6) as

$$\hat{\sigma}(A) = N_{90}\exp(-x(A^{\frac{1}{3}} - 90^{\frac{1}{3}})), \tag{7}$$

where N_{90}, the unit cross section at $A = 90$, and x are adjustable parameters. The error distribution of each data point was assumed to be a Gaussian, while the standard deviation is the quadratic sum of four uncertainties: (1) uncertainties in the cross sections due to peak fitting, beam current, and target thicknesses, (2) uncertainties in the B(GT) values, (3) estimation of the contribution from the low-lying multipole excitations to the cross sections for the ^{118,120}Sb(g.s.), and (4) effect of the contaminant material in the ^{118}Sn target. Figures 8 and 9 show the A-dependences at 198 and 297 MeV, respectively, where the shaded areas indicate one standard deviation in the A-dependences due to the parameter adjustment. If one eliminates the problematic $\hat{\sigma}_{\rm GT}$ datum of ^{114}Cd in the

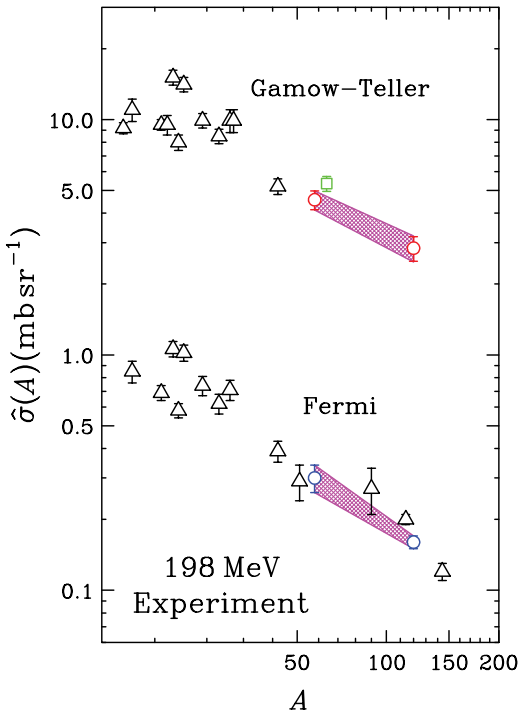

FIG. 8. (Color online) Unit cross sections $\hat{\sigma}_{GT,F}$ vs. A at 198 MeV. Open circles are our data. Open triangles are from data by Taddeucci *et al.* [10]. Open square is from the datum of the (n,p) reaction by Williams *et al.* [6]. Shaded areas show the A-dependences of the unit cross sections with 1σ uncertainty.

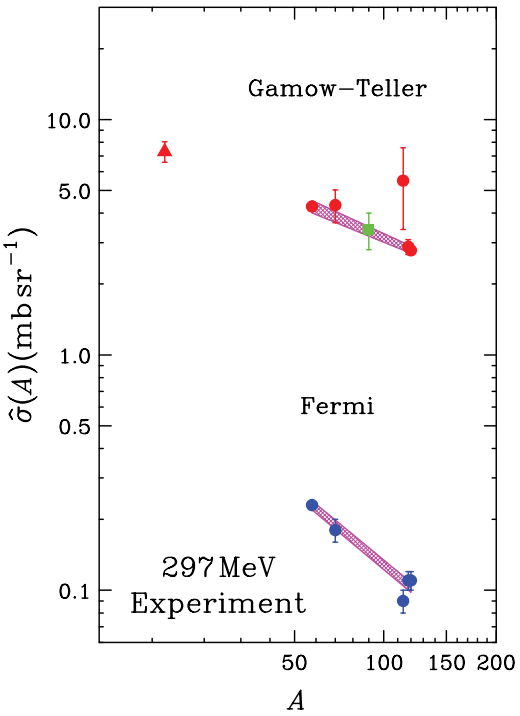

FIG. 9. (Color online) Unit cross sections $\hat{\sigma}_{GT,F}$ vs. A at 297 MeV. Filled circles are our data. Filled triangles are from data by Watson *et al.* [31]. Filled square is the $\hat{\sigma}_{GT}$ value for ^{90}Zr used in Ref. [5]. Shaded areas show the A-dependences of the unit cross sections with 1σ uncertainty. See the text for the reliability of the $\hat{\sigma}_{GT}$ value of ^{114}Cd.

parameter adjustment of the $\hat{\sigma}_{GT}$ A-dependence at 297 MeV, the x_{GT} and N_{90} values would change only by <0.1%.

Table III summarizes the obtained parameters in Eq. (7). Taddeucci *et al.* have studied the energy dependence of the slope parameter x_{GT} by the DWIA calculations and found that x_{GT} decreases from 0.54 to 0.42 as the energy increases from $T_p = 120$ MeV to 200 MeV [10]. The x_{GT} value of 0.45 ± 0.14 obtained in this work at 198 MeV agrees well with their value. In addition, the x_{GT} value decreases further to 0.40 ± 0.05 at 297 MeV due to increasing nuclear opacity in the energy region approaching 300 MeV [11].

The square symbol in Fig. 9 is the $\hat{\sigma}_{GT}$ value of 3.5 ± 0.6 mb/sr for ^{90}Zr at 297 MeV used in Ref. [5], which discussed B(GT) in the continuum. The authors of Ref. [5] have estimated this value by comparing the sum of the GT cross sections up to the GTGR region of $E_x < 16$ MeV to the corresponding GT transition strength deduced by systematic (p,n) measurements at 160 MeV [3] after correcting for the energy dependence. The present A-dependence of 297 MeV provides a $\hat{\sigma}_{GT}$ value of 3.36 ± 0.17 mb/sr. Herein the error is the quadratic sum of the uncertainty due to the determination of the A-dependence (±3%) and other systematic uncertainties (±4%), which are not used to derive the A-dependence. It is interesting that the value in Ref. [5] is fairly close to the present value. If the present $\hat{\sigma}_{GT}$ value is used in the analysis in Ref. [5], the quenching factor of GT spin sum rule, Q, becomes $0.92 \pm 0.06 \pm 0.05$ instead of $0.88 \pm 0.06 \pm 0.16$ [5]. The error due to $\hat{\sigma}_{GT}$ is significantly reduced from ±0.16 to ±0.05.

TABLE III. Parameters for the A-dependence of $\hat{\sigma}_{GT,F}$ at 198 and 297 MeV.

	N_{90} (mb/sr)	x_{GT}	N_{90} (mb/sr)	x_F
198 MeV	3.5 ± 0.3	0.45 ± 0.14	0.21 ± 0.02	0.6 ± 0.1
297 MeV	3.4 ± 0.2	0.40 ± 0.05	0.14 ± 0.01	0.8 ± 0.1

The open square in Fig. 8 is the $\hat{\sigma}_{GT}$ value of 5.3 ± 0.4 mb/sr obtained from the ^{64}Ni$(n,p)^{64}$Co reaction at 200 MeV [6]. This value has been used to normalize the B(GT) distributions in ^{60,62,64}Co [6], which are important for calculating the reaction rate of electron captures in a stellar core before super novae [7,8]. However, this value is 20% larger than that estimated from the present A-dependence at 198 MeV, 4.3 ± 0.4 mb/sr. The difference between Ref. [6] and this work could be due to the contribution from the 0.3-MeV GT state in ^{64}Co, which is observed by the β^--decay measurement of ^{64}Fe [32] and by the ^{64}Ni$(t,^3$He$)^{64}$Co measurement [33]. As discussed in Ref. [6], the $(t,^3$He) result suggests that the contribution of this state is 22% of the "g.s. peak" in Ref. [6].

B. A-dependence of R^2

The R^2 values obtained from the present data of $\hat{\sigma}_{GT}$ and $\hat{\sigma}_F$ are summarized in Table I and are shown as a function of A by

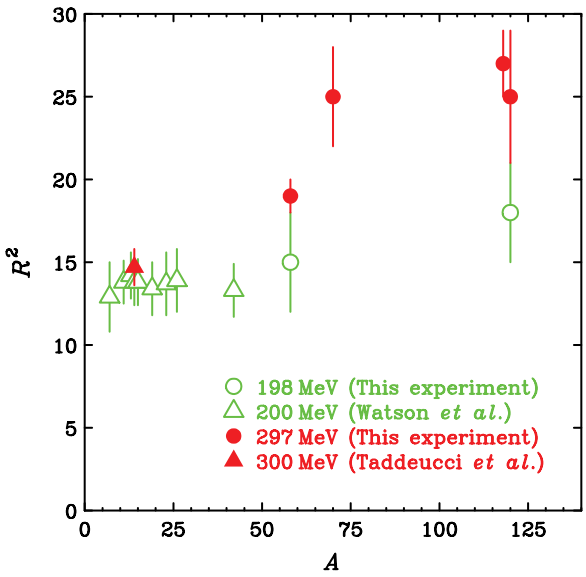

FIG. 10. (Color online) R^2 vs. A. Open circles are our data at 198 MeV. Open triangles are the previous data at 200 MeV by Taddeucci *et al.* [10]. Filled circles are our data (excluding ^{114}Cd) at 297 MeV. Filled triangles are the previous data at 300 MeV by Alford *et al.* [34].

circles in Fig. 10. The error bar of each data point is the result of the quadratic sum of the uncertainties due to the fitting and B(GT).

Figure 10 also plots the existing R^2 values for light nuclei up to ^{42}Ca at 200 and 300 MeV taken from Refs. [10] and [34], respectively, as triangles. Compared with them, the present R^2 values for the heavier nuclei are found to be large. In addition, as expected from the difference between $x_{\rm GT}$ and $x_{\rm F}$ in Table III, R^2 increases with the increasing of A in the mass region heavier than ^{42}Ca. It should be noted that R^2 is almost independent of A below ^{42}Ca [10]. A similar trend exists for previously reported R^2 values from the (^{3}He,t) measurements at 140 MeV per nucleon [35].

V. SUMMARY AND CONCLUSION

We measured the (p,n) reaction on medium-heavy nuclei, ^{58}Ni, ^{70}Zn, ^{114}Cd, ^{118}Sn, and ^{120}Sn at 0° at 198 and 297 MeV to determine the GT and Fermi unit cross sections as well as their ratios (R^2). The A-dependence of the unit cross sections was deduced, which is helpful in deducing B(GT) values from (p,n) cross sections. It is notable that the $\hat{\sigma}_{\rm GT}$ value at $A = 90$ interpolated from the present A-dependence at 297 MeV is almost equal to the value estimated from the data at 160 MeV, which was used in the analysis of the ^{90}Zr(p,n) experiment [4] to determine the quenching of the GT spin sum rule. However, the present $\hat{\sigma}_{\rm GT}$ value at $A = 64$ and $T_p = 198$ MeV is 20% smaller than that used in the analysis of ^{60,62,64}Ni(n,p) spectra at 200 MeV [6]. The present R^2 values in the mass region heavier than ^{42}Ca are larger than the known values in the region up to ^{42}Ca, and increase as A increases.

ACKNOWLEDGMENTS

We are grateful to the accelerator group of RCNP for their efforts to provide a high quality proton beam, which is indispensable for a good energy resolution. The experiments were performed at RCNP, Osaka University under the Experimental Program No. E218. This work was supported by a Grant-in-Aid for Specially Promoted Research No. 17002003 of the Ministry of Education, Culture, Sports, Science, and Technology of Japan.

[1] F. Osterfeld, Rev. Mod. Phys. **64**, 491 (1992).
[2] M. Ichimura, H. Sakai, and T. Wakasa, Prog. Nucl. Phys. **56**, 446 (2006).
[3] C. Gaarde, J. Rapaport, T. N. Taddeucci, C. D. Goodman, C. C. Foster, D. E. Bainum, C. A. Goulding, M. B. Greenfield, D. J. Horen, and E. Sugarbaker, Nucl. Phys. **A369**, 258 (1981).
[4] T. Wakasa, H. Sakai, H. Okamura, H. Otsu, S. Fujita, S. Ishida, N. Sakamoto, T. Uesaka, Y. Satou, M. B. Greenfield, and K. Hatanaka, Phys. Rev. C **55**, 2909 (1997).
[5] K. Yako, H. Sakai, M. B. Greenfield, K. Hatanaka, M. Hatano, J. Kamiya, H. Kato, Y. Kitamura, Y. Maeda, C. L. Morris, H. Okamura, J. Rapaport, T. Saito, Y. Sakemi, K. Sekiguchi, Y. Shimizu, K. Suda, A. Tamii, N. Uchigashima, and T. Wakasa, Phys. Lett. **B615**, 193 (2005).
[6] A. L. Williams, W. P. Alford, E. Brash, B. A. Brown, S. Burzynski, H. T. Fortune, O. Häusser, R. Helmer, R. Henderson, P. P. Hui, K. P. Jackson, B. Larson, M. G. McKinzie, D. A. Smith, A. Trudel, and M. Vetterli, Phys. Rev. C **51**, 1144 (1995).
[7] M. C. Vetterli, K. P. Jackson, A. Celler, J. Engel, D. Frekers, O. Häusser, R. Helmer, R. Henderson, K. H. Hicks, R. G. Jeppesen, B. Larson, B. Pointon, A. Trudel, and S. Yen, Phys. Rev. C **45**, 997 (1992).
[8] W. P. Alford, B. A. Brown, S. Burzynski, A. Celler, D. Frekers, R. Helmer, R. Henderson, K. P. Jackson, K. Lee, A. Rahav, A. Trudel, and M. C. Vetterli, Phys. Rev. C **48**, 2818 (1993).
[9] K. Langanke and G. Martinez-Pinedo, Rev. Mod. Phys. **75**, 819 (2003).
[10] T. N. Taddeucci, C. A. Goulding, T. A. Carey, R. C. Byrd, C. D. Goodman, C. Gaarde, J. Larsen, D. Horen, J. Rapaport, and E. Sugarbaker, Nucl. Phys. **A469**, 125 (1987).
[11] Qing-biao Shen, Da-chun Feng, and Yi-zhong Zhuo, Phys. Rev. C **43**, 2773 (1991).
[12] Z. Janas, M. Karny, Y. Fujita, L. Batist, D. Cano-Ott, R. Collatz, P. Dendooven, A. Gadea, M. Gierlik, M. Hellström, Z. Hu, A. Jokinen, R. Kirchner, O. Klepper, F. Moroz, M. Oinonen, H. Penttilä, A. Plochocki, E. Roeckl, B. Rubio, M. Shibata, J. L. Tain, and V. Wittman, Eur. Phys. J. A **12**, 143 (2001).
[13] J. K. Tuli, Nucl. Data Sheets **103**, 389 (2004).
[14] J. Blachot, Nucl. Data Sheets **97**, 593 (2002).
[15] K. Kitao, Nucl. Data Sheets **75**, 99 (1995).
[16] K. Kitao, Nucl. Data Sheets **96**, 241 (2002).

[17] T. Wakasa, Y. Hagaihara, M. Sasano, S. Asaji, K. Fujita, K. Hatanaka, T. Ishida, T. Kawabata, H. Kuboki, Y. Maeda, T. Noro, T. Saito, H. Sakai, Y. Sakemi, K. Sekiguchi, Y. Shimizu, A. Tamii, Y. Tameshige, and K. Yako, Nucl. Instrum. Methods Phys. Res. A **547**, 569 (2005).
[18] H. Sakai, H. Okamura, S. Ishida, K. Hatanaka, and T. Noro, Nucl. Instrum. Methods Phys. Res. A **320**, 479 (1992).
[19] T. N. Taddeucci, W. P. Alford, M. Barlett, R. C. Byrd, T. A. Carey, D. E. Ciskowski, C. C. Foster, C. Gaarde, C. D. Goodman, C. A. Goulding, E. Gülmez, W. Huang, D. J. Horen, J. Larsen, D. Marchlenski, J. B. McClelland, D. Prout, J. Rapaport, L. J. Rybarcyk, W. C. Sailor, E. Sugarbaker, and C. A. Whitten Jr., Phys. Rev. C **41**, 2548 (1990).
[20] B. Singh, Nucl. Data Sheets **87**, 177 (1999).
[21] J. Gulyas, T. Fényes, F. M. Hassan, Zs. Dombrádi, J. Kumpulainen, and R. Julin, Phys. Rev. C **46**, 1218 (1992).
[22] R. Schaeffer and J. Raynal, Program DW70 (unpublished); J. Raynal, Nucl. Phys. **A97**, 572 (1967); J. R. Comfort, extended version DW81 (unpublished).
[23] M. A. Franey and W. G. Love, Phys. Rev. C **31**, 488 (1985).
[24] S. Hama, B. C. Clark, E. D. Cooper, H. S. Sherif, and R. L. Mercer, Phys. Rev. C **41**, 2737 (1990).
[25] A. Bohr and B. R. Mottelson, *Nuclear Structure*, (Benjamin, New York, 1969), Vol. 1, p. 239.
[26] Y. Fujita and T. Adachi (private communication).
[27] I. S. Towner and J. C. Hardy, Phys. Rev. C **77**, 025501 (2008).
[28] W. M. Yao *et al*. (Particle Data Group), J. Phys. G **33**, 1 (2006).
[29] L. Grodzins and H. Motz, Phys. Rev. **102**, 761 (1956).
[30] N. B. Gove and M. J. Martin, Nucl. Data Tables **10**, 205 (1971).
[31] J. W. Watson *et al*., Phys. Rev. C **40**, 22 (1989).
[32] E. Runte, K. L. Gippert, W. D. Schmidt-Ott, P. Tidemand-Petersson, L. Ziegeler, R. Kirchner, O. Klepper, P. O. Larsson, E. Roeckl, D. Schardt, N. Kaffrell, P. Peuser, M. Bernas, P. Dessagne, M. Langevin, and K. Rykaczewski, Nucl. Phys. **A441**, 237 (1985).
[33] E. R. Flynn and J. D. Garrett, Phys. Lett. **B42**, 49 (1972).
[34] W. P. Alford, R. L. Helmer, R. Abegg, A. Celler, O. Häusser, K. Hicks, K. P. Jackson, C. A. Miller, S. Yen, R. E. Azuma, D. Frekers, R. S. Henderson, H. Baer, and C. D. Zafiratos, Phys. Lett. **B179**, 20 (1986).
[35] Y. Fujita, J. Phys. Conf. Ser. **20**, 107 (2005).